

E4S: Fine-grained Face Swapping via Editing With Regional GAN Inversion

Maomao Li^{1*}, Ge Yuan^{2*}, Cairong Wang³, Zhian Liu⁴, Yong Zhang^{5†}, Yongwei Nie⁴,
Jue Wang, and Dong Xu^{1†},

¹ The University of HongKong ² Sun Yat-sen University ³Tsinghua Shenzhen International Graduate School
⁴ South China University of Technology ⁵Tencent AI Lab

Abstract—This paper proposes a novel approach to face swapping from the perspective of fine-grained facial editing, dubbed “*editing for swapping*” (E4S). The traditional face swapping methods rely on global feature extraction and often fail to preserve the source identity. In contrast, our framework proposes a Regional GAN Inversion (RGI) method, which allows the explicit disentanglement of shape and texture. Specifically, our E4S performs face swapping in the latent space of a pre-trained StyleGAN, where a multi-scale mask-guided encoder is applied to project the texture of each facial component into regional style codes and a mask-guided injection module then manipulates feature maps with the style codes. Based on this disentanglement, face swapping can be simplified as style and mask swapping. Besides, since reconstructing the source face in the target image may lead to disharmony lighting, we propose to train a re-coloring network to make the swapped face maintain the lighting condition on the target face. Further, to deal with the potential mismatch area during mask exchange, we designed a face inpainting network as post-processing. The extensive comparisons with state-of-the-art methods demonstrate that our E4S outperforms existing methods in preserving texture, shape, and lighting. Our implementation is available at <https://github.com/e4s2023/E4S2023>.

1. Introduction

Face swapping aims at not only transferring the identity information (e.g., shape and texture of facial components) of a source face to a given target face, but also keeping the identity-irrelevant attribute information unchanged (e.g., expression, head pose, lighting, and background, etc.). It has broad masses of potential applications in movie composition, computer games, and virtual human broadcasting, thus attracting considerable attention in the field of computer vision and graphics.

Early face-swapping works [4], [5] attempt at pixel-level manipulation for exchanging inner face regions, sometimes with the help of 3D facial models to handle the pose difference between the two input faces [6], [7]. These methods typically have difficulties in preserving the target

facial attributes (e.g., expression) [4] and the source identity [7]. Recent methods [1], [8], [9], [10] employ Generative Adversarial Networks (GAN) [11] to achieve high fidelity swapping results. Although continuous efforts have been pursued, there are two long-standing challenges in face swapping that remain unsolved, as we will elaborate next.

The first challenge is **identity preservation**, *i.e.*, making the swapped results faithfully preserve the facial characteristics of the source person. Most mainstream approaches [8], [9], [10] extract the global identity-related features and inject them into the face generation process, where these identity features are obtained via a pre-trained 2D face recognition network [12] or a 3D morphable face model (3DMM) [13], [14]. Nonetheless, these methods always exhibit the “in-between effect” and struggle to present satisfying results. Concretely, their swapped result looks like a third person, which resembles both the source and target faces. Here, we argue the potential reason is current identity extractors are mainly designed for classification rather than generation, thus cannot capture some informative and important facial visual details. Moreover, when a 3D face model takes one single image as input, it can hardly achieve precise shape recovery robustly.

The second challenge is how to deal with **facial occlusion**. It is common that some face regions are occluded by hair (or eyeglasses) in the input images. An ideal swapped result should maintain the hair (or eyeglasses) of the target. That is, it needs to generate the occluded facial regions for the source face. To deal with occlusion, FSGAN [15] trains an inpainting sub-network to generate the missing pixels of the source. However, their inpainted faces are blurry. FaceShifter [9] designs a refinement network to recover the occluded region in the target. Nonetheless, the refinement network always brings back certain identity information of the target to the source image.

Although past efforts have achieved promising results, the above challenges still pose the main obstacles that prevent fine-grained face swapping. Here comes to a question that can we build a face swapping framework to handle the aforementioned challenges at once? In this paper, we will explore such feasibility. Specifically, we propose to rethink face swapping from a new perspective of fine-grained face editing, *i.e.*, “*editing for swapping*” (E4S). The key insight

• * *Eual contribution*, † *Corresponding authors*.

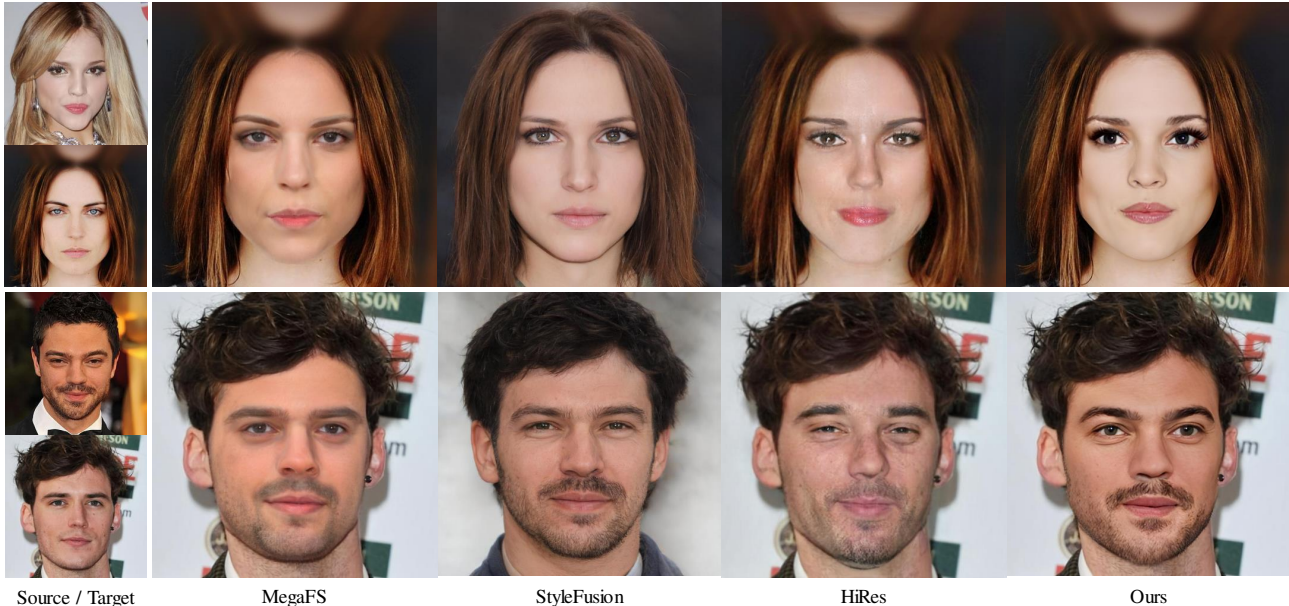


Figure 1: Compared with the existing StyleGAN-based face swapping approaches MegaFS [1], StyleFusion [2], and HiRes [3], our E4S can achieve high-fidelity swapped results. Note that ours achieves best identity preservation and proper occlusion handling, where the target skin tone is kept and the target lighting condition is well transferred to the swapped results. All the facial images are at 1024×1024 .

behind this is that given the disentangled shape and texture of individual facial components from two faces, face swapping can be transformed into the problem of local shape and texture replacement between them.

Inspired by the previous fine-grained face editing approach [16], we apply separated component masks for local feature extraction. Then, we recompose local shapes and textures, which are fed into a mask-guided generator to synthesize the swapped result. Before conducting shape and texture swapping, we use a face reenactment model [17] to drive the source person to have the same pose and expression as the target. The unique advantage of our E4S framework is that the facial occlusion challenge can be naturally addressed by facial masks since the face parsing network [18] can provide labels of each face region. Our mask-guided generator can fill out the swapped masks with the swapped texture features adaptively. It does not rely on additional dedicated modules as in previous efforts [9], [15].

Given that StyleGAN [19] has achieved striking performance on high-quality image editing, the core of our E4S framework is taking advantage of a pre-trained StyleGAN [19] for the disentanglement of shape and texture. This is a demanding mission, since the existing GAN inversion methods [20], [21], [22] only performs global attribute editing (*e.g.*, age, gender, and expression) in the global style space of StyleGAN, and does not throw any glance on local shape and texture editing. To achieve this goal, we propose a novel Regional GAN Inversion (RGI) method that incorporates facial masks into style embedding and introduces a regional \mathcal{W}^+ space, indicated as \mathcal{W}^{r+} . Specifically, we design a mask-guided multi-scale encoder that maps an input face into the style space of StyleGAN, where we

make each facial component have a set of style codes for different layers of the generator. Besides, based on given facial masks, a mask-guided injection module is proposed, which uses style codes to manipulate the feature maps in the generator. That is, the disentanglement of texture and shape is conducted by using style codes and masks to represent them, respectively. With such disentanglement, fine-grained face swapping can be achieved by flexibly swapping the style codes and masks of all facial components.

During the mask-exchange process, it is difficult to obtain a perfect recomposed mask for the swapped face, especially when the face shapes of source and target are very different. For example, when source’s face is thin and target’s face is fat, some mismatched facial mask regions need to be replaced by background, neck, or hair, etc. In this paper, we propose to train a face inpainting network as post-processing, where we form the paired data by erasing the mismatched area from the source as the before-inpainting data, and using the original source as the after-inpainting data. During inference, guided by those mismatched mask regions, the inpainting network can generate swapped results which meet the face shape of the source.

Besides shape and texture, we argue that lighting is also crucial for face swapping. If the lighting condition of the source and target is extremely different, it will be unnatural to combine the source face and the surrounding ambient from the target. To deal with this, inspired by Hesser [23], we reformulate the lighting-transferring problem as conducting face re-coloring from its corresponding grayscale images. Concretely, we train a face re-coloring network in a self-supervised manner. It is trained by paired data with the same identity, where one is a grayscale face while the other

is the corresponding colored face. Note that skin tone and lighting are entangled, the results of our face re-coloring network would maintain the skin of the target, nonetheless, which is more practical in real face swapping application. In summary, the main contributions of this paper are:

- We propose E4S, a fine-grained face swapping framework from a new perspective of face editing. Our high-fidelity face swapping is capable of preserving source identity and target lighting and dealing with occlusion challenge.¹
- We propose a Regional GAN Inversion (RGI) method for the explicit disentanglement of shape and texture based on a pre-trained StyleGAN.
- we train a face re-coloring network, making the lighting of the swapped result be faithful to the target.
- To solve the mismatch area that may occur in the process of mask exchange, we additionally designed a face inpainting network for post processing for E4S.
- Extensive quantitative and qualitative results demonstrate that our E4S and RGI exceeds current state-of-the-art face swapping methods.

2. Related Work

GAN Inversion. There have been various approaches proposed for GAN inversion, which aim to map an image to its corresponding latent code that can faithfully reconstruct the input. Such methods are useful for image editing, as the inverted code can be modified and then fed into the generator to produce the desired output. Existing approaches for StyleGAN inversion can be broadly categorized into three groups: learning-based [21], [22], [24], [25], [26], [27], optimization-based [28], [29], [30], [31], [32], and hybrid methods [33]. Learning-based methods involve training an encoder to map the image to the latent space, whereas optimization-based methods directly optimize the latent code to minimize the reconstruction error. Although optimization-based methods tend to yield better results, they are more computationally expensive than learning-based methods. Hybrid methods seek to balance these two approaches by using the inverted code as a starting point for further optimization.

Existing GAN inversion methods always perform global editing, allowing for modifications such as changes in pose, gender, and age. However, they cannot precisely control local facial features. To address this limitation, we utilize Regional GAN Inversion, which employs a novel \mathcal{W}^r latent space based on a pre-trained StyleGAN. This new approach enables high-fidelity local editing of facial components, filling an important gap in existing methods. Face Swapping. Face-swapping approaches can be broadly categorized into two classes: source-oriented and target-oriented [8]. Source-oriented methods [15], [34], [35], [36],

[37] initiate from the source, aiming to transfer the target’s attributes to it. Early techniques in this category can be traced back to [34], which estimated 3D shape and relevant scene parameters for pose and lighting alignment. Later, [36] claimed that 3D shape estimation was unnecessary and applied face segmentation for face swapping. Recently, FSGAN [15], [37] employed a two-stage pipeline where a reenactment and inpainting network addressed pose alignment and occlusion issues, respectively. As contrast, target-oriented methods [8], [9], [10], [38], [39], [40], [41] start with the target, intending to import the source identity. Generally, these approaches maintain the source identity using a pre-trained face recognition model or 3DMMs. However, as the recognition model is trained for classification and 3DMMs lack accuracy and robustness, these methods fail to fully capture identity-related details for generation, resulting in the ”in-between effect”.

Regarding StyleGAN-based face swapping, MegaFS [1] leverages prior knowledge from the pre-trained StyleGAN, increasing image resolution to 1024². StyleFusion [2] performs latent fusion within the \mathcal{S} space [42], [43], allowing for controllable generation of local semantic regions. Nonetheless, the shape and texture of each facial region remain entangled in the \mathcal{S} space. In contrast, [40] proposes a region-aware projector for adaptively transferring source identity to the target face. HiRes [3] utilizes an additional encoder-decoder for multi-scale target feature aggregation, but these two techniques do not support fine-grained and selective swapping.

Our *E4S* belongs to the source-oriented group. Taking inspiration from mask-guided face editing [16], [44], [45], [46], we reframe face swapping as editing shape and texture for all facial components. We propose to explicitly disentangle facial components’ shape and texture using the RGI method for better identity preservation, instead of relying on a face recognition model or 3DMMs.

3. Method

In this section, we first introduce our proposed editing-for-swapping (E4S) framework and elaborate on each inside step in Sec. 3.1. Then, we explain the proposed region GAN inversion (RGI) method for the disentanglement of the shape and texture of facial components in Sec. 3.2. Each core module of the RGI is detailed subsequently. Next, we introduce the face recoloring network B_ψ for maintaining the target skin tone and lighting, and the face inpainting network P_τ for the unnatural results caused by the possible shape mismatch during mask exchange in Sec. 3.3. After that, we present the loss functions for training in Sec. 3.4.

3.1. Editing For Swapping (E4S) framework

Given an arbitrary pair of source and target faces, our goal is to generate a swapped face that retains the identity information from the source and keeps the identity-irrelevant attributes (*e.g.*, pose, expression, lighting and background)

1. The implementation is at <https://github.com/e4s2023/E4S2023>. The project page is available at <https://e4s2023.github.io/>.

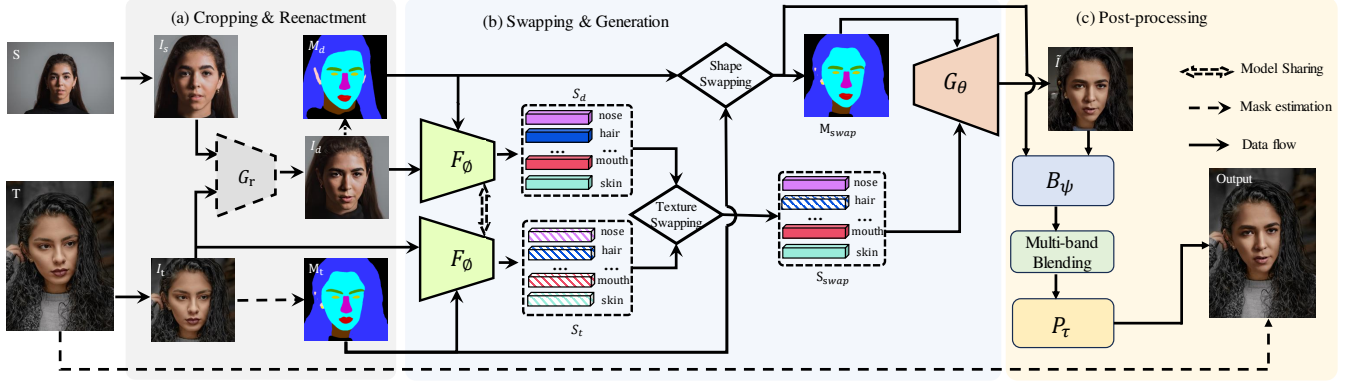


Figure 2: E4S framework overview. (a) We first crop the face region of the source S and the target T to obtain I_s and I_t . Then, a reenactment network G_r encourages I_s to have a similar pose and expression towards I_t , obtaining the driven image I_d . The segmentation masks of I_t and I_d are also estimated. (b) Then, the driven and target pairs (I_d, M_d) and (I_t, M_t) are fed into the mask-guided encoder F_ϕ to extract the per-region style codes to depict the texture respectively, producing texture codes S_d and S_t . Next, we exchange the masks and the corresponding texture codes, and send them to the pre-trained StyleGAN generator G_θ with a mask-guided injection module to synthesize the naive swapped face \tilde{I} . (c) Finally, we conduct post-processing, which includes a face re-coloring network B_ψ for transferring the target lighting to \tilde{I} , multi-band blending for pasting back the swapped face to T , and a face inpainting network P_τ for preserving an inconsistent shape with source face.

from the target. The pipeline of our face swapping framework is illustrated in Fig. 2, which mainly consists of three phases inside: (a) cropping and reenactment, (b) swapping and generation, and (c) post-processing.

3.1.1. Cropping and Reenactment. We first crop the face region of the source image S and target image T respectively, obtaining the cropped faces I_s and I_t , which can be expressed as:

$$I_s = f_c(S), \quad I_t = f_c(T), \quad (1)$$

where f_c denotes the cropping processing. We use the `dlib`² toolbox to crop the face region and detect the facial landmarks. Then, we follow the previous method [47] to align the cropped face and resize it into 1024×1024 resolution.

To drive I_s to obtain the similar pose and expression as I_t , we employ a pre-trained face reenactment model FaceVid2Vid [17], obtaining a driven face I_d . The face reenactment processing can be expressed as:

$$I_d = G_r(I_s, I_t), \quad (2)$$

where G_r is the FaceVid2Vid model. Then, the segmentation masks M_t of the target face I_t and M_d of the driven face I_d are estimated by an off-the-shell face parser [48]. In this way, the target and driven pairs (I_t, M_t) and (I_d, M_d) can be formed, where each segmentation mask belongs to one of the 19 semantic categories. For brevity, we aggregate the categories of symmetric facial components, bringing 12 categories totally, *i.e.*, *background, eyebrows, eyes, nose, mouth, lips, face skin, neck, hair, ears, eyeglass, and ear rings*.

3.1.2. Swapping and Generation. After the cropping and reenactment process, we are ready to fulfil the face swapping process. We first feed the driven pair (I_d, M_d) and the target pair (I_t, M_t) into a mask-guided multi-scale encoder F_ϕ respectively, obtaining the style codes to represent the texture of each facial region. This step can be described as:

$$S_t = F_\phi(I_t, M_t), \quad S_d = F_\phi(I_d, M_d), \quad (3)$$

where S_t and S_d denote the extracted texture codes of the target and driven face, respectively. The detailed modules of the encoder F_ϕ are introduced in Sec. 3.2. Then, we exchange the texture codes of several facial components of S_t with those of S_d , resulting in the recomposed texture codes S_{swap} . The components that must be exchanged are: *eyebrows, eyes, nose, mouth, lips, face, skin, neck, and ears*. One may be confused about the exchange of *skin*, since this paper aims to maintain the skin tone and lighting of the target. The reason we use the *skin* component from the source is replacing the texture codes of skin from the source face with the target one can not bring satisfactory results. Thus, we turn to a skin recoloring network for post-processing, rather than keeping the skin color of the target directly in the swapping process.

To achieve face swapping, besides of texture swapping, shape swapping is also needed. Considering face shape can be indicated by facial masks, we start with an empty mask M_{swap} as a canvas and then complete the mask recombination. Specifically, we first keep the neck and the background from the target mask M_t and stitch their masks onto M_{swap} . Next, we stitch the inner face regions of the driven mask M_d , including *face skin, eyebrows, eyes, nose, lips, and mouth*. Finally, we stitch the *hair, eye glasses, ear, and ear rings* from the target mask M_t to the M_{swap} .

2. <http://dlib.net/>

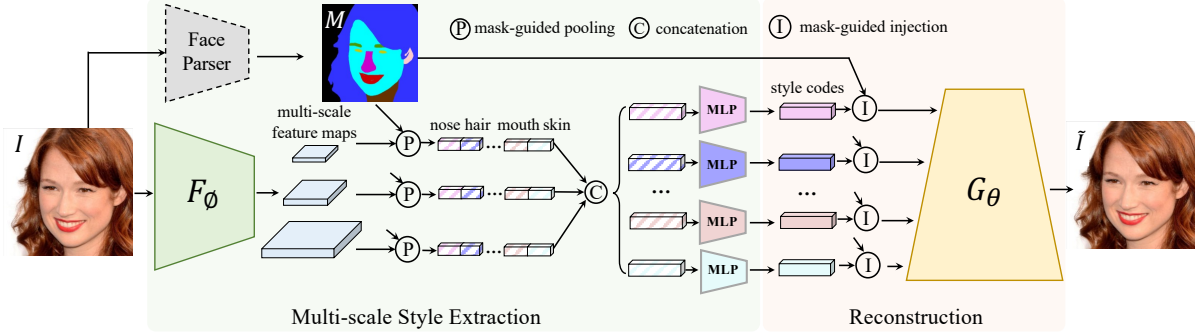


Figure 3: Overview of the proposed RGI. The input face I together with the corresponding segmentation map M are fed into a multi-scale encoder F_ϕ to extract the per-region texture vectors. The multi-scale texture vectors are then concatenated and passed through some MLPs to get the style codes resident in the latent space of StyleGAN. The regional style codes and the mask M are used by our mask-guided StyleGAN generator to produce the reconstructed face \tilde{I} .

Next, we feed the recomposed mask M_{swap} and texture codes S_{swap} into the StyleGAN generator G_θ with a mask-guided style injection module to synthesize the swapped face I , which can be described as:

$$\tilde{I} = G_\theta(M_{\text{swap}}, S_{\text{swap}}). \quad (4)$$

The details of the generator G_θ will be introduced in the Sec. 3.2. Note that our E4S does not need to train an extra sub-network to deal with the occlusion and can naturally achieve more accurate occlusion recovery than the existing methods FSGAN [15] and FaceShifter [9]. This is because the generator G_θ can fill out the occlusion pixels with the swapped texture features adaptively according to masks.

3.1.3. Post-Processing. Since the disentanglement of texture and shape solely cannot guarantee a lighting-natural swapped result, we additionally propose a face-recoloring network B_ψ to conduct transferring of skin and lighting from the target face I_t to the swapped face \tilde{I} , which is elaborated in Sec. 3.3.1. Then, the swapped face \tilde{I} and target image T are blended together via Multi-Band Blending, producing the naive final swapped image F_{final} , which is detailed in Sec. 3.3.2. Finally, considering that the potential mismatch during the mask recombination process of M_d and M_t would cause difficulty for the shape keeping of source face, we propose an inpainting network P_τ , which operates on pixel level and maintain the source face shape by the guide of mismatched region masks. we give the detailed description of the inpainting network P_τ in the Sec. 3.3.3.

3.2. Disentangling Shape and Texture

The key insight for the proposed E4S framework is disentangling the per-region texture and its corresponding shapes. To pursue a better disentanglement of shape and texture as well as the high-resolution and high-fidelity generation, we resort to the powerful generative model StyleGAN that can generate images with 1024×1024 resolution naturally. Specifically, we aim to develop a GAN inversion method rather than training StyleGAN from scratch. That

is, we leverage a pre-trained StyleGAN for the disentanglement, which also avoids training instability.

Although there are quite a few GAN inversion methods [21], [24], [26] have been proposed for face editing in the style space, they constantly focus on global facial attribute editing (eg, age, pose, expression, etc.) and do not pay attention to disentanglement of shape and texture for local editing. To fill this gap, we propose a novel Regional GAN Inversion (RGI) method for such a disentanglement, which incorporates facial masks into the style embedding and the generation process. The overview of RGI is in Fig. 3.

3.2.1. Mask-guided Style Extraction. Assuming there is an image I and its segmentation mask M , we first leverage a multi-scale encoder F_ϕ to take the image I as input and produce feature maps at different levels as:

$$[F_1, F_2, \dots, F_N] = F_\phi(I), \quad (5)$$

where N represents the number of scales and F_ϕ indicates a convolution network with multiple layers. Then, the multi-scale features for each individual facial region can be obtained via the feature maps $[F_1, F_2, \dots, F_N]$ and the mask M . Concretely, we downsize the mask M to the same scale with each feature map F_i , and then use the average pooling operation on F_i to aggregate features for each facial region:

$$v_{ij} = \text{Average}(F_i \odot (\lfloor M \rfloor_i == j)), \forall j \in \{1, 2, \dots, C\}, \quad (6)$$

where C denotes the number of segmentation categories, \odot represents the Hadamard product, and $\lfloor M \rfloor_i$ indicates the downsized mask with the same size as F_i . Further, we concatenate the multi-scale feature vectors $\{v_{ij}\}_{i=1}^N$ of the region j and put them into an MLP, thus obtaining the style codes, which can be described as:

$$s_j = \text{MLP}([v_{1j}; v_{2j}; \dots; v_{Nj}]), \quad (7)$$

where s_j indicates the style codes of the j -th facial region. Then, the generator G_θ takes as input the style codes and the mask M are fed into the generator to generate the swapping result. Formally, we define $s \in \mathbb{R}^{C \times 18 \times 512}$ as the proposed \mathcal{W}^{r+} space.

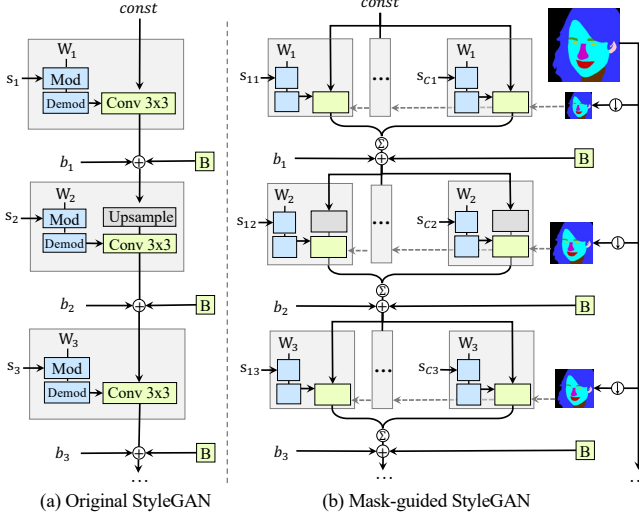


Figure 4: Detailed comparison of the original StyleGAN and the proposed mask-guided StyleGAN. (a) The original StyleGAN contains consecutive convolution blocks. Each block contains a modulation, a demodulation, and a convolution layer. The W and b denote the learnable kernel weights for each block, and s denotes the style code. The \boxed{B} stands for noise broadcast operation. An upsampling layer is used between every two blocks. (b) Our mask-guided StyleGAN regionally extends the convolution block. We sum up the intermediate feature maps of each region according to its segmentation mask which is downsized in advance.

3.2.2. Mask-guided Style Injection. The original StyleGAN contains a style-based generator taking 18 style codes with the dimension of 512 as input. The style codes are used to manipulate the feature maps of the 18 intermediate layers. As shown in Fig. 4 (a), the generator, consisting of a serial of style blocks, takes a constant feature map with the spatial size of 4×4 as input. Each style block includes a modulation, a demodulation, 3×3 convolution layer, and a noise layer \boxed{B} used to increase the diversity. Here, the learnable kernel weights and bias in each block are denoted as W and b , respectively. W would be scaled by its corresponding style code s with the shape of 1×512 before the convolution layer. An additional upsampling layer by the factor of two is adopted between every two style blocks, increasing the resolution of feature maps.

In this paper, we aim to extract regional style code that controls the local appearance of the corresponding face component precisely along with its mask, which is opposite to the way of style code in the original StyleGAN, which globally controls the appearance of the output image. To achieve this, we overhaul the style block of the original StyleGAN to a mask-guided style block, which is based on a given mask. Fig. 4 (b) illustrates the schematic operations of our proposed mask-guided style injection. Specifically, we sum up the intermediate feature maps with the guidance

of per-region mask as:

$$F_l = \sum_{j=1}^C (F_{l-1} * W'_{jl}) \odot (\lfloor M \rfloor_l == j), \forall l \in \{1, 2, \dots, K\}, \quad (8)$$

$$W'_{jl} = \text{Demod}(\text{Mod}(W_l, s_{jl})), \quad (9)$$

where F_{l-1} and F_l indicate the input and output feature maps of l -th layer, separately. W'_{jl} represents the scaled kernel weights for the j -th component in the l -th layer, and $*$ denotes the convolution operation. Similar to Eq. 6, the $\lfloor M \rfloor_l$ is the downsized mask corresponding to the l -th layer. Following the same modulation and demodulation as the original StyleGAN, we extend the style modulation regionally. In Eq. 9, W_l denotes the original kernel weights for the l -th layer, and the s_{jl} indicates the style code of j -th component for the l -th layer.

It is worth noticing that we only inject the mask into the first K layers of the StyleGAN and do not use the mask-guided style block for the last $(18 - K)$ layers. The reason here is twofold: (i) we experimentally find that the reconstructed images have few visual differences when K is greater than 13; (ii) since the resolution of the last $(18 - K)$ layers is large (*i.e.*, $512^2 - 1024^2$), the training cost would be lowered when mask-guided style injection is not conducted in these layers. Thus, we set $K = 13$ as the default in all the experiments.

The previous work SofGAN [46] is similar to our mask-guided StyleGAN since both of us regionally extend the style modulation. However, SofGAN applies an extra encoding module to map the mask M to a $4 \times 4 \times 512$ feature map. In contrast, we resort to the pretrained StyleGAN constant instead. Besides, SofGAN leverages spatially adaptive normalization [44] in the intermediate layers to strengthen the influence of the segmentation maps, while ours does not need since we find our region-aware convolution can already control the layout of each facial component well.

3.3. Post-Processing for Natural Lighting and Face-Shape Consistency

Although the E4S framework can provide a unique face swapping insight (*i.e.*, disentangling shape and texture), there are still some situations that it cannot handle well.

- (i) When the lighting difference between source and target is huge, reconstructing the face of source in the ambient lighting of target would produce disharmonious results.
- (ii) Directly using alpha-blending to blend the swapped face \tilde{I} and target T would lead to cliff edges, resulting in unnatural appearance in border area (*e.g.*, hairline).
- (iii) During the process of generating the recomposed mask M_{swap} , there would inevitably be some unmatched mask regions. For instance, for those positions belong to the inner face of the target, but not to that of the source, to maintain the shape of the source, these unmatched face regions should be injected with the style code of non-inner face category (hair, neck, etc.). However, different unmatched

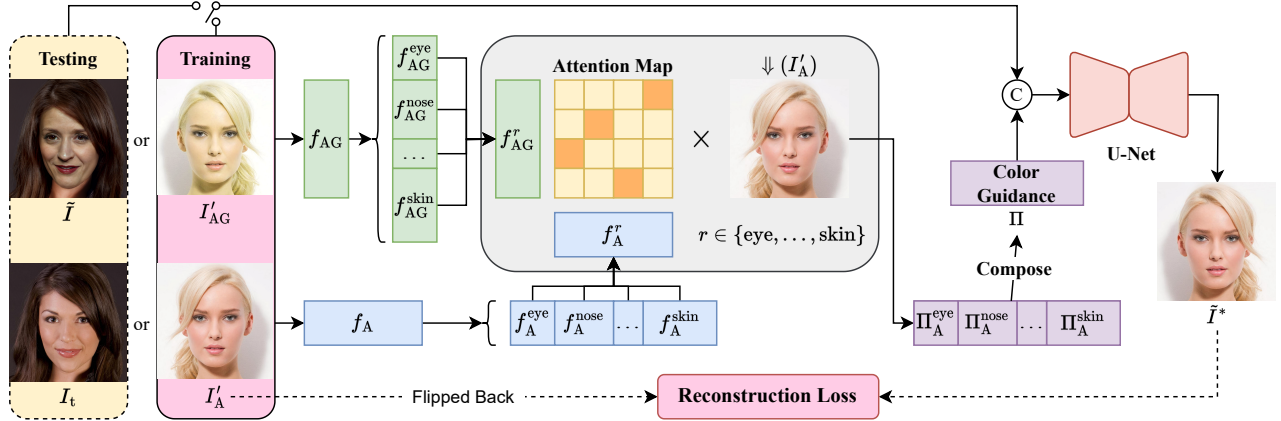


Figure 5: Illustration of our re-coloring network B_ψ . In the training stage, we use two image augmentation to obtain the random re-colored I'_{AG} and flipped I'_A . Then, we apply FPN [49] to acquire corresponding features f_{AG} and f_A , where the feature of same semantic region in f_{AG} and f_A are used to calculate attention maps. Next, we multiply the maps with the downsampled I'_A to generate color guidance for each semantic region. Consequently, the composed color guidance Π , input images I'_{AG} and I'_A and their segmentation masks are concatenated through channel dimension and together fed to a U-Net to generate the re-colored result \tilde{I}^* . In the testing stage, given the swapped face \tilde{I} to be recolored and the cropped target I_t providing color conditions, B_ψ can transfer the color from I_t to \tilde{I} , resulting in the re-colored swapped result \tilde{I}^* .

regions may correspond to different injected style codes. Furthermore, even if the mismatch regions are injected with the correct style code and yield a perfect recomposed mask M_{swap} , guided by this mask, the content generated in the mismatch regions tends to conflict with the original target image T . It brings difficulty for conducting blending on the reconstructed image \tilde{I} and target T .

To address the above issues, we additionally provide three post-processing techniques for more fine-grained and lighting-consistent face swapping, which consist of: transferring lighting condition and skin tones from the target to the swapped result with an additional face re-colorer B_ψ , Multi-Band Blending on the recolored image \tilde{I}^* and non-cropped target T , and training an additional inpainting network P_r to restore mismatch-mask regions.

3.3.1. Face Re-coloring. Preserving the target lighting condition is a challenging task, especially when the illumination of the source is leaked into the result. Disentangling the illumination requires recovering material, geometry, and lighting of a scene, making this issue ill-posed. To deal with the re-lighting challenge, we reformulate the re-lighting problem as a re-coloring problem and propose to transfer the color from the target to the swapped face by our re-colorer B_ψ . Although the swapped face color should be determined by both the source skin tone and target environment lighting, we simplify the re-lighting problem by transferring the target color to the swapped face. In practice, we found this simplification leads to reasonable and admirable results, improving the result fidelity, as shown in Fig. 8.

However, it is impossible to collect annotated paired data for the training of transferring the color of a reference face to the objective face. It may take great expense and huge labor to manually paint reasonable output. Thus, inspired

by HeSer [23], we turn to perform self-supervised training, where we set the face to be colored and the reference face as the same identity during training. Specifically, for a given RGB face I_A , we convert it into a grayscale image I_{AG} . As seen in Fig. 5, we first conduct random color augmentation CA on the grayscale image I_{AG} and a random horizontal flip augmentation FA on the original image I_A respectively:

$$I'_{AG} = \text{CA}(I_{AG}), I'_A = \text{FA}(I_A), \quad (10)$$

The reason for using additional flip augmentation is to prevent the network from copying the pixels from the same position directly. Then, we obtain feature representation of I'_{AG} and I'_A using feature pyramid network FPN [49]:

$$\begin{aligned} f_{AG} &= \text{FPN}(I'_{AG}) \in \mathbb{R}^{N \times C}, \\ f_A &= \text{FPN}(I'_A) \in \mathbb{R}^{N \times C}, \end{aligned} \quad (11)$$

where C indicates the number of channels and N is the spatial zone of features. The next step is to compute the correlations between extracted features in each spatial location. Specifically, we calculate the correlations among the same semantic region in facial mask M_t , avoiding correlation calculation among those uncorrelated regions. The process can be expressed as:

$$S^r = f_{AG}^r f_{A^T}^r \in \mathbb{R}^{N^r \times N^r}. \quad (12)$$

where f_{AG}^r and f_A^r are the corresponding feature of each region $r \in \{\text{eyebrows, eyes, nose, mouth, lips, face, and skin}\}$. S^r indicates pair-wise correlation of each facial region, and $S_{i,j}^r$ is similarity between i -th pixel in f_{AG}^r and j -th pixel in f_A^r . N_r denotes the number of pixels of each region. Next, the correlation matrix S^r is normalized by softmax layer

and then multiplied with the pixels of downsampled I'_A in region r , which can be expressed as:

$$\Pi^r = \frac{S^r}{\sum_{j=1}^{N^r} S^r_{:,j}} (\Downarrow(I'_A)^r) \in \mathbb{R}^{N^r \times 3}, \quad (13)$$

where Π^r denotes the color guidance in region r , and $\Downarrow(\cdot)$ indicates the downsampling operation. Combining all the Π^r , we can obtain the full facial color guidance $\Pi \in \mathbb{R}^{N \times 3}$. Then, we concatenate the representation I'_{AG} , I'_A , upsampled color guidance $\Uparrow(\Pi)$, and the semantic segmentation mask M_A (omitted in Fig. 5) of I_A , and pass them to train a recoloring UNet, where $\Uparrow(\cdot)$ indicates the upsampling operation. Our goal here is to distill color from the colored image I'_A to I'_{AG} . Once this re-colorer B_ψ is trained, we can transfer the color of the target I_t to \tilde{I} as:

$$\tilde{I}^* = B_\psi(\tilde{I}, M_d, I_t, M_t), \quad (14)$$

where M_d and M_t are semantic segmentation masks of the swapped face \tilde{I} and target I_t , respectively.

Furthermore, since the high computational cost of calculating cosine similarity in 1024×1024 resolution (e.g. calculating cosine similarity matrix between the *skin* parts of two 1024×1024 faces requires 64GB memory in average), we train the U-Net in 256×256 resolution. Although the memory is more efficient, the produced 256 recoloring result looks very blur when we directly resize it to 1024×1024 resolution. Therefore, we use a face super-resolution method [50] to enhance the low-resolution result and paste the enhanced recolored image to \tilde{I} based on a low-pass mask where the high-frequency pixels is removed by a Sobel filter, as shown in Fig. 8.

3.3.2. Multi-Band Blending. It is a natural choice to use Alpha Blending to blend the recolored swapped face \tilde{I}^* and target image T as the naive final swapped image I_α , which can be expressed as:

$$I_\alpha = \tilde{I}^* * M_{\text{swap}}^{\text{inner}} + T * (1 - M_{\text{swap}}^{\text{inner}}), \quad (15)$$

where $M_{\text{swap}}^{\text{inner}}$ indicates the inner face area of the swapped face \tilde{I}^* . However, such a result would have a stiff splice on the border of the inner face area (e.g., hairline). To deal with this, we use Multi-Band Blending [51], [52] to paste the swapped face \tilde{I}^* back to the original target T . Multi-Band Blending conducts image smoothing in the low-frequency band and image sharpening in the high-frequency band. The Multi-Band Blending process can be formulated as:

$$\tilde{I}^*_{\text{paste}} = \text{MBB}(\tilde{I}^*, T, M_{\text{swap}}^{\text{inner}}) \quad (16)$$

where $\text{MBB}(\cdot)$ denotes the Multi-Band Blending algorithm. Concretely, a typical Multi-Band Blending algorithm consists of three steps: building image pyramids, blending computation, and reconstruction. Multi-Band Blending is able to seamlessly blend two images in a given mask region (i.e. $M_{\text{swap}}^{\text{inner}}$ in our case).

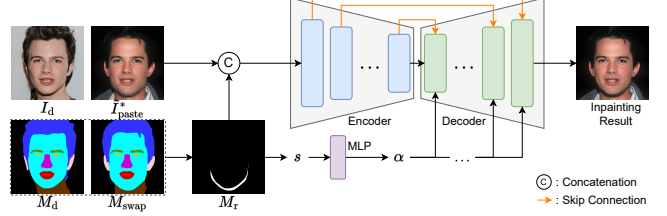


Figure 6: Illustration of inpainting network P_τ , which adaptively inpaints the mismatch regions on the pixel levels. Given a driven face I_d and the pasted $\tilde{I}^*_{\text{paste}}$, we first calculate the mismatch regions mask M_r . Then the image $\tilde{I}^*_{\text{paste}}$ along with the mismatch mask M_r are fed to an auto-encoder to inpaint the mismatch pixels. The generation process of the decoder is modulated by a vector α extracted from the area ratio s of mismatch regions.

3.3.3. Inpainting For Mismatch-mask Region. There would inevitably be quite a few mismatched regions during facial mask exchange between the driven face M_d and target M_t (Sec. 3.1). Here, we divide facial mask into two categories: inner face region (*eyebrows, eyes, nose, mouth, lips, face, and skin*) and non-inner face region (*neck, ears, hair, earrings, and background*). Then, there are two types of face mismatched pixels in the recomposed mask M_{swap} : 1) the positions belong to the inner face of the source, but not to that of the target; 2) the positions belong to the inner face of the target, but not to that of the source. In the first case, to keep face shape of the source, we directly use face mask of the source to fill those mismatched positions. For the second case, we need to fill the position with a proper non-inner face category. In this paper, we define a mismatched region M_r as the second case since it cannot be solved directly:

$$M_r = \{(x, y) | M_d^{\text{inner}}[x, y] = 0 \ \& \ M_t^{\text{inner}}[x, y] = 1\}, \quad (17)$$

where M_d^{inner} indicates the inner face region of driven face mask, M_t^{inner} denotes the inner face region of target mask.

A natural idea to solve the mismatched region is to design an algorithm to adaptively arrange each position in the region with a proper non-inner face category (e.g., nearest neighbour classifier). However, we empirically notice that even if all mismatched regions are filled with the correct category, guided by this perfect recomposed mask, the content generated in this region tends to conflict with the original target image T . This is because some background information should be generated in those locations which once belonged to the face area. Such conflict would lead to disharmony at the borders of the mismatched region after Multi-Band Blending. Thus, this paper turns to train an inpainting network P_τ that fills the mismatched region in the blended result $\tilde{I}^*_{\text{paste}}$ in the pixel-level rather than the mask-level.

The details of the face-inpainting network P_τ are shown in Fig. 6. We detail the training process in the Appendix. During inference, given the pasted $\tilde{I}^*_{\text{paste}}$ and the driven source I_d , the mismatch regions M_r of these two faces is calculated by Eqn. 17. Then the inpainting network P_τ re-

covers the erased content, producing a refined result sharing the consistent face shape with the source. Then the area ratio (ranging in $[0, 1]$) of mismatch regions (white parts of M_r in Fig. 6) is fed to an MLP, extracting a vector α which modulates the generation process of the decoder. We only copy the inpainted pixels lying in mismatched regions to the input. Consequently, the network P_r is capable of preserving the facial shape of the source without additionally seeking a perfect recomposed mask M_{swap} .

3.4. Training Objective

Different from the most current face swapping methods, our E4S takes reconstruction as the proxy task, making it easy to train. When training is finished, one can employ the texture encoder F_ϕ to generate per-region texture codes for any input face. Then, face swapping can be easily fulfilled as described in Sec. 3.1. We apply the commonly used loss functions in the GAN inversion methods, which are detailed in our Appendix, where the training objectives of the face re-coloring network B_ψ and face inpainting network P_r are also presented.

4. Experiment Setup

4.1. DataSets.

CelebAMask-HQ [16] consists of 30K high-quality face images, which can be split into 28k and 2K for training and testing, separately. The dataset provides the facial segmentation masks, which has 19 semantic categories in total.

FFHQ [47] contains 70K high-quality at 1024^2 resolution. It includes vastly variation in terms of age, ethnicity and image background, and also has better coverage of accessories such as eyeglasses, sunglasses, hats, etc. Since it does not provide the facial segmentation masks, we use a pre-trained face parser [48] to obtain the facial segmentation masks.

4.2. Implementation Details.

The proposed RGI is trained with PyTorch [53] with 8 NVIDIA Tesla A100 GPUs. The batch size is 2 at each GPU during training. The learning rate is initialized as 10^{-4} with the Adam [54] optimizer ($\beta_1 = 0.9$, $\beta_2 = 0.999$). We train the model for 200K and 300K iterations on CelebAMask-HQ and FFHQ datasets, respectively. Besides, The initial learning rate decays by the factor of 0.1 at 100K and 150K iterations, separately. Here, all images are randomly flipped with a ratio of 0.5. As for the adversarial training, we update the parameters of the discriminator once the generator gets updated 15 times. The reason here is that the pre-trained StyleGAN can well preserve the texture details of inner face components, while sometimes its performance is unstable on preserving the hair details. Hence, we finetune the first $K = 13$ layers to improve the hair quality. As for the RGI-Optimization, we fix the learning rate as $1e^{-2}$. Empirically, approximately 50 steps of optimization would bring satisfying results.

TABLE 1: Quantitative comparison of our RGI under different ablative configurations. The reconstruction performance is measured.

| Configurations | SSIM \uparrow | PSNR \uparrow | RMSE \downarrow | FID \downarrow |
|--------------------|-----------------|-----------------|-------------------|------------------|
| our RGI full model | 0.818 | 19.851 | 0.105 | 15.032 |
| (A) w/o finetuning | 0.827 | 19.984 | 0.104 | 22.239 |
| (B) w/o MS encoder | 0.817 | 19.732 | 0.107 | 15.112 |

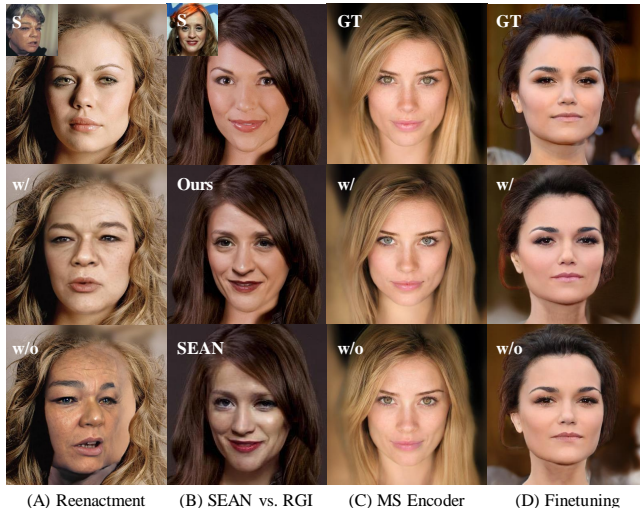


Figure 7: Qualitative comparisons of different ablative settings.

We train the re-coloring network and inpainting network on 256×256 images sampled from CelebAMask-HQ and FFHQ. Both of the networks are optimized by Adam [54] with $\beta_1 = 0.9$ and $\beta_2 = 0.999$.

5. Ablation study.

We perform ablation studies on the different parts of the proposed E4S framework. All the ablative experiments are conducted on the CelebAMask-HQ dataset. We provide the quantitative comparison under different RGI configurations in Table 1, where the reconstruction performance is considered. Besides, the qualitative ablation comparison in E4S is shown in Fig. 7.

The Role of Re-enactment. We first study the roles of re-enactment step of E4S framework, which aims to drive the source to show a similar pose and expression as the target. However, aside from pose and expression, an ideal reenactment model should not affect other source attributes, such as identity. Specifically, we employ a pre-trained face reenactment model [17] before the shape and texture swapping procedure. To verify the necessity of the re-enactment step in E4S, we compare a standard E4S pipeline and the one without re-enactment. As shown in the 1st column of Fig. 7, the swapped result is not aligned with the target face when the reenactment is disabled.

SEAN vs RGI. Our E4S is a general model. Specifically, if there is a method which contains an encoder extracting the per-region style codes and a generator controlling the per-region style codes along with the segmentation mask, it

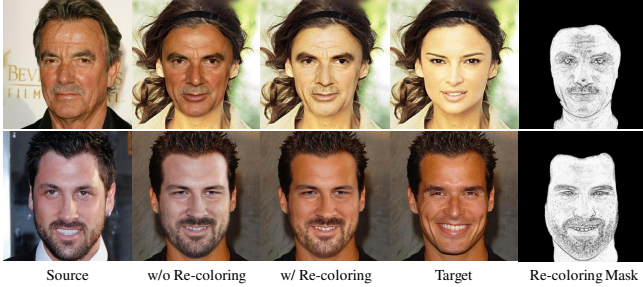


Figure 8: Qualitative results of ablation study on face re-coloring (zooming in for more details).

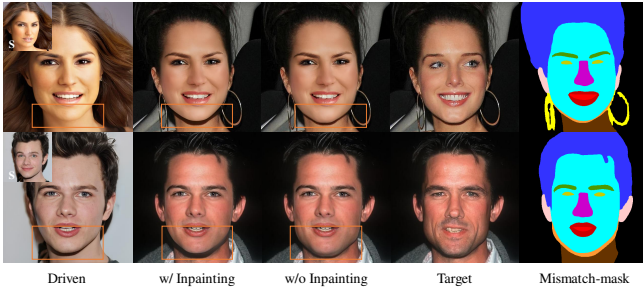


Figure 9: Qualitative results of ablation study on face inpainting (zooming in for more details).

can be adapted to our E4S framework. To prove this, we replace our RGI with SEAN [45] to play the roles of F_ϕ and G_θ . It can be observed from the 2nd column of Fig. 7, our results preserve details better (e.g., hair texture, hair color, tone, and overall identity), whereas SEAN sometimes produces artifacts in the hair region. Besides, SEAN only demonstrates its ability to generate faces at 256^2 while ours are at 1024^2 . Both of these two findings show the superiority of our RGI.

Multi-scale vs single-scale encoder. We also study the role of the multi-scale encoder in configuration (B), where only the last level of feature maps produced by F_ϕ is used. Compared with our baseline, the performance of the single-scaled encoder is worse, which is consistent with the qualitative comparison shown in the 3rd column in Fig. 7 (see the color of eyes). This demonstrates that the multi-scale encoder can improve the quality of generated images.

Pre-trained vs fine-tuned StyleGAN. The pre-trained StyleGAN can be used for face swapping. However, we notice that the hair texture details cannot be always well preserved. For a more robust performance on hair, we fine-tune the first $K = 13$ layers of the StyleGAN. In Table 1, we use a configuration (A) to indicate freezing the parameters of the StyleGAN generator and only training the texture encoder F_ϕ and the subsequent MLPs in our RGI. Although better SSIM, PSNR, and RMSE can be achieved by (A), the FID is poor. The last column in Fig. 7 also supports this. As contrast, fine-tuning can improve hair quality while maintaining the texture of other inner facial components. The generated images look unrealistic and lack certain tex-

tures (especially in hair). The generation quality can also be proved by the higher FID.

The Role of face re-coloring network B_ψ . To evaluate the performance of the proposed face re-coloring network B_ψ , we provide the qualitative results in Fig. 8. The comparison results demonstrate that using re-coloring network can produce more natural and target-consistent lighting. Besides, although B_ψ only generates 256^2 -resolution images, the final re-coloring results have the comparable image quality with the 1024^2 sized inputs, with the help of face enhancing network [50] restoring the details and re-coloring mask preserving the high-frequency information.

The Role of face inpainting network P_τ . We also study the role of face inpainting network P_τ in Fig. 9. This clearly shows that as post-processing, network P_τ can successfully and adaptively keep the face shape of the source, even though the face-shape difference between source and target is extremely large. Besides, the quantitative comparison between our standard E4S and the one without face re-coloring network B_ψ or face inpainting network P_τ are demonstrated in Table 2. We would elaborate on this in Sec. 6.2.

6. Face Swapping Results.

We first illustrate several face swapping examples synthesized by our E4S framework and several representative methods in Fig. 10. Our method can realize high-quality swapping at the resolution of 1024×1024 . Then, we compare our method with the previous StyleGAN-based face swapping works in Fig. 11. Next, we randomly sample 500 source-target pairs from the test set of CelebAMask-HQ to obtain the swapped results of different approaches. Besides, we provide video face swapping results in Appendix. Moreover, we develop a user-interface system to perform image and video face swapping, which are also detailed in Appendix.

6.1. Qualitative comparison.

We provide the qualitative comparisons with state-of-the-art methods in Fig. 10, where our E4S achieves more realistic and high-fidelity swapped results than the others. Compared with FSGAN [15], our results are much sharper. The results of SimSwap [8] and Hiface [10] suffer from some artifacts and distortions (see the 2nd and 4th row). Although both our E4S and FaceShifter [9] can generate visually-satisfying results, ours shows better detailed textures.

We further compare the performance in more challenging cases where the occlusion exists in the source and target faces (see the last two rows in Fig. 10). It can be observed that our E4S can fill out the missing skin in the source face (see the last row), and preserve the target glasses (see the 3rd row). As contrast, FSGAN results are quite blurry although they design a dedicated inpainting sub-network for occlusion. FaceShifter proposes a refinement network to maintain the occlusion in the target image, which also may



Figure 10: Qualitative comparisons of our results with state-of-the-art face swapping methods. Our method can achieve high-fidelity results, which preserves the identity from the source better (*e.g.*, beard, eyes, face shape) and attribute condition from the target (*e.g.*, lighting and background). Note that our E4S maintain the skin tone from the target which is more practical in face swapping application. Best viewed in color and zoom-in.



Figure 11: Comparisons with StyleGAN-based face swapping methods.

bring back some identity information of the target, making the identity of their swapped results confused.

We also compare with some StyleGAN-based approaches in Fig. 11. The results of MegaFS [1] look to be a mixture of the source and target, which are blurry and lack of textures. StyleFusion [2] shows a bit of over-smoothing (see the last row). HiRes [3] still suffer from some artifacts in 1024^2 resolution. As contrast, our E4S can generate more realistic and high-quality face swapping results.

TABLE 2: Quantitative comparison with the existing face swapping methods. we denote the best results with **bold** marks. †: source-oriented method, ‡: target-oriented method, *: StyleGAN-based method.

| Method | ID retrieval↑ | | Pose↓ | Expr.↓ |
|--------------------------|---------------|-------------|-------------|-------------|
| | Top-1 | Top-5 | | |
| † FSGAN [15] | 0.17 | 0.32 | 2.33 | 2.45 |
| ‡ SimSwap [8] | 0.12 | 0.32 | 2.89 | 2.84 |
| ‡ FaceShifter [9] | 0.06 | 0.26 | 1.73 | 2.35 |
| ‡ HifiFace [10] | 0.15 | 0.37 | 2.77 | 2.82 |
| * MegaFS [1] | 0.29 | 0.45 | 3.03 | 3.05 |
| * StyleFusion [2] | 0.35 | 0.18 | 5.37 | 2.94 |
| ‡ * HiRes [3] | 0.05 | 0.51 | 2.71 | 2.83 |
| † * Our E4S w/o B_ψ | 0.40 | 0.57 | 3.29 | 3.07 |
| † * Our E4S w/o P_τ | 0.38 | 0.55 | 3.28 | 3.06 |
| † * Our standard E4S | 0.42 | 0.58 | 3.28 | 3.05 |

6.2. Quantitative comparison.

The quantitative comparison is listed in Table 2. It considers two aspects: *identity preservation* from the source and the *attribute preservation* from the target. Specifically, inspired by FaceShifter, our experimental settings are as follows. For source identity preservation, we first extract the ID feature vectors of all the source faces and the swapped results via CosFace [55]. Then, we conduct face retrieval by searching for the most similar face from all the

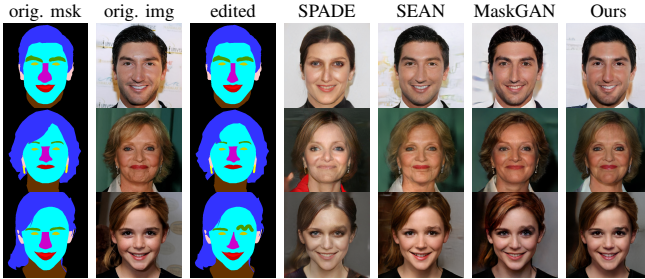


Figure 12: Qualitative comparisons of our results with state-of-the-art face editing methods. Some modifications are made on the face contour, hair, nose, and eyebrows. Our method can produce more high-fidelity editing results while maintaining the details of other components and the overall identity information well.

source images for each swapped face, where the similarity is computed as the cosine distance. We use Top-1 and Top-5 accuracy as the evaluation metrics. For the target attribute preservation, we estimate the pose and expression by using HopeNet [56] and a 3D face reconstruction model [14], respectively. The ℓ_2 distance of the pose and expression between each swapped face and its ground-truth target face is used as metrics.

Table 2 shows our E4S achieves the best retrieval accuracy, which demonstrates the superiority of our method on identity preservation. As for the target attribute preservation, our E4S achieves comparable results in pose and expression. In general, the target-oriented methods usually keep more accurate pose and expression, since they start from the target face while our E4S is a source-oriented method, which generates the target attributes starting from the source. Nonetheless, one side effect of the target-oriented methods is that the injected identity information from the source is always limited (see FaceShifter in Fig. 10 and HiRes in Fig. 11). To sum up, there is a trade-off between identity and attribute preservation in source- and target-oriented methods. Note that our E4S has the potential to achieve better results by leveraging a more advanced reenactment method.

Besides, we also evaluate how the proposed face recoloring network B_ψ and face inpainting network P_τ make a difference to the overall E4S framework in Table 2. Although the face re-coloring network B_ψ basically does not affect the performance on source ID retrieval and target pose and expression, it totally changes the visual effects of human eyes since the face skin tone is maintained from the target rather the source (see Fig. 8). Besides, Fig. 9 has demonstrated the proposed face inpainting network P_τ can successfully maintain the face shape, which cannot be solved well by mask-swapping only. The quantitative comparison in Table 2 demonstrates our face inpainting network P_τ can improve the performance of ID retrieval since accurately maintaining source face shape is important for source ID retrieval. Such a performance improvement is consistent with the results in Fig. 9.

TABLE 3: Quantitative comparison for image reconstruction on CelebAMask-HQ [16] test set. The rows in gray indicate the reconstruction images are obtained via style code optimization.

| method | SSIM \uparrow | PSNR \uparrow | RMSE \downarrow | FID \downarrow |
|------------------|-----------------|-----------------|-------------------|------------------|
| SPADE [44] | 0.64 | 15.67 | 0.17 | 20.45 |
| SEAN [45] | 0.71 | 18.57 | 0.12 | 17.74 |
| MaskGAN [16] | 0.75 | 19.42 | 0.11 | 19.03 |
| Our RGI | 0.82 | 19.85 | 0.10 | 15.03 |
| sofGAN [46] | 0.76 | 14.86 | 0.19 | 26.73 |
| RGI-Optimization | 0.86 | 23.02 | 0.07 | 14.73 |

7. Face Editing Results Via RGI.

Other than face swapping, our RGI can also be used for fine-grained face editing. Here, we make a comparison with our method and the current state-of-the-art fine-grained face editing works: SPADE [44], Mask-guided GAN [57], SEAN [45], and MaskGAN [16]. To present a fair comparison, we train our RGI on the training set of CelebAMask-HQ and evaluate it on the test set.

7.1. Qualitative comparison.

We show the visual comparison with the competing methods in Fig. 12. We make some modifications to the original facial mask, such as hair, eyebrows, and face contour. It shows that our approach produces more high-fidelity editing results, where the details of other components and the overall identity information are well kept.

7.2. Quantitative comparison.

We make comparison between the competing methods and our RGI on the image reconstruction quality, where the Structural Similarity Index (SSIM) [58], Root-Mean-Squared-Error (RMSE), Peak Signal-to-Noise Ratio (PSNR), and Fréchet Inception Distance (FID) [59] are used as the metrics. The results are showed in Table 3. We also compare E4S with SofGAN [46], which is a StyleGAN-based method and takes style code optimization for the reconstruction. For a fair comparison, we use RGI-Optimization. Table 3 shows that our method always achieves the best performance on all metrics, indicating the superiority of our method. SEAN [45] sometimes produces artifacts on hair regions while our RGI can achieve more high-fidelity reconstructions with better identity, texture, and illumination. Besides, our RGI-Optimization can preserve the facial details better (*e.g.*, the curly degree of hair, the thickness of the beard, dimples, and background).

8. Conclusion

In this paper, we present a novel framework E4S for face swapping, which considers conducting face swapping from the perspective of fine-grained face editing, *i.e.*, “*editing*”

for swapping”. Our E4S proposes to explicitly disentangle the shape and texture of each facial component, thus the face swapping task can be reformulated as a simplified problem of texture and shape swapping. To achieve such disentanglement as well as high resolution and high fidelity, we propose a novel Regional GAN inversion (RGI) method. Specifically, a multi-scale mask-guided encoder is designed to project the input face into the per-region style codes, which are resident in the style space of StyleGAN. Besides, we design a mask-guided injection module that uses the style codes to manipulate the feature maps in the generator according to the given masks. Besides of shape of texture, we propose to transfer the target lighting to the swapped face by training a face re-coloring network, which is trained in a self-supervised manner to recover the corresponding grayscale images. Further, as a post-processing, we design a face inpainting network to maintain the source face shape on the pixel level. We conduct extensive experiments on face swapping, face editing and some extended applications. The results and comparisons with current state-of-the-art methods demonstrate the superiority of the E4S framework, RGI method, face re-coloring and face inpainting network.

References

- [1] Y. Zhu, Q. Li, J. Wang, C.-Z. Xu, and Z. Sun, “One shot face swapping on megapixels,” in *Proceedings of the IEEE/CVF Conference on Computer Vision and Pattern Recognition*, 2021, pp. 4834–4844. [1](#), [2](#), [3](#), [11](#)
- [2] O. Kafri, O. Patashnik, Y. Alaluf, and D. Cohen-Or, “Stylefusion: A generative model for disentangling spatial segments,” *arXiv preprint arXiv:2107.07437*, 2021. [2](#), [3](#), [11](#)
- [3] Y. Xu, B. Deng, J. Wang, Y. Jing, J. Pan, and S. He, “High-resolution face swapping via latent semantics disentanglement,” in *Proceedings of the IEEE/CVF Conference on Computer Vision and Pattern Recognition*, 2022, pp. 7642–7651. [2](#), [3](#), [11](#), [17](#), [18](#)
- [4] D. Bitouk, N. Kumar, S. Dhillon, P. Belhumeur, and S. K. Nayar, “Face swapping: automatically replacing faces in photographs,” in *ACM SIGGRAPH 2008 papers*, 2008, pp. 1–8. [1](#)
- [5] H.-X. Wang, C. Pan, H. Gong, and H.-Y. Wu, “Facial image composition based on active appearance model,” in *2008 IEEE International Conference on Acoustics, Speech and Signal Processing*. IEEE, 2008, pp. 893–896. [1](#)
- [6] V. Blanz, K. Scherbaum, T. Vetter, and H.-P. Seidel, “Exchanging faces in images,” in *Computer Graphics Forum*, vol. 23, no. 3. Wiley Online Library, 2004, pp. 669–676. [1](#)
- [7] Y. Nirkin, I. Masi, A. T. Tuan, T. Hassner, and G. Medioni, “On face segmentation, face swapping, and face perception,” in *2018 13th IEEE International Conference on Automatic Face & Gesture Recognition (FG 2018)*. IEEE, 2018, pp. 98–105. [1](#)
- [8] R. Chen, X. Chen, B. Ni, and Y. Ge, “Simswap: An efficient framework for high fidelity face swapping,” in *Proceedings of the 28th ACM International Conference on Multimedia*, 2020, pp. 2003–2011. [1](#), [3](#), [10](#), [11](#)
- [9] L. Li, J. Bao, H. Yang, D. Chen, and F. Wen, “Faceshifter: Towards high fidelity and occlusion aware face swapping,” *arXiv preprint arXiv:1912.13457*, 2019. [1](#), [2](#), [3](#), [5](#), [10](#), [11](#), [17](#), [18](#)
- [10] Y. Wang, X. Chen, J. Zhu, W. Chu, Y. Tai, C. Wang, J. Li, Y. Wu, F. Huang, and R. Ji, “Hififace: 3d shape and semantic prior guided high fidelity face swapping,” *arXiv preprint arXiv:2106.09965*, 2021. [1](#), [3](#), [10](#), [11](#)
- [11] I. Goodfellow, J. Pouget-Abadie, M. Mirza, B. Xu, D. Warde-Farley, S. Ozair, A. Courville, and Y. Bengio, “Generative adversarial nets,” *Advances in neural information processing systems*, vol. 27, 2014. [1](#)
- [12] J. Deng, J. Guo, N. Xue, and S. Zafeiriou, “Arcface: Additive angular margin loss for deep face recognition,” in *Proceedings of the IEEE/CVF conference on computer vision and pattern recognition*, 2019, pp. 4690–4699. [1](#), [16](#)
- [13] V. Blanz and T. Vetter, “A morphable model for the synthesis of 3d faces,” in *Proceedings of the 26th annual conference on Computer graphics and interactive techniques*, 1999, pp. 187–194. [1](#)
- [14] Y. Deng, J. Yang, S. Xu, D. Chen, Y. Jia, and X. Tong, “Accurate 3d face reconstruction with weakly-supervised learning: From single image to image set,” in *Proceedings of the IEEE/CVF Conference on Computer Vision and Pattern Recognition Workshops*, 2019, pp. 0–0. [1](#), [12](#)
- [15] Y. Nirkin, Y. Keller, and T. Hassner, “Fsgan: Subject agnostic face swapping and reenactment,” in *Proceedings of the IEEE/CVF international conference on computer vision*, 2019, pp. 7184–7193. [1](#), [2](#), [3](#), [5](#), [10](#), [11](#)
- [16] C.-H. Lee, Z. Liu, L. Wu, and P. Luo, “Maskgan: Towards diverse and interactive facial image manipulation,” in *Proceedings of the IEEE/CVF Conference on Computer Vision and Pattern Recognition*, 2020, pp. 5549–5558. [2](#), [3](#), [9](#), [12](#), [16](#)
- [17] T.-C. Wang, A. Mallya, and M.-Y. Liu, “One-shot free-view neural talking-head synthesis for video conferencing,” in *Proceedings of the IEEE/CVF Conference on Computer Vision and Pattern Recognition*, 2021, pp. 10 039–10 049. [2](#), [4](#), [9](#)
- [18] C. Yu, C. Gao, J. Wang, G. Yu, C. Shen, and N. Sang, “Bisenet v2: Bilateral network with guided aggregation for real-time semantic segmentation,” *International Journal of Computer Vision*, vol. 129, no. 11, pp. 3051–3068, 2021. [2](#)
- [19] T. Karras, S. Laine, M. Aittala, J. Hellsten, J. Lehtinen, and T. Aila, “Analyzing and improving the image quality of stylegan,” in *Proceedings of the IEEE/CVF conference on computer vision and pattern recognition*, 2020, pp. 8110–8119. [2](#)
- [20] Y. Shen, C. Yang, X. Tang, and B. Zhou, “Interfacegan: Interpreting the disentangled face representation learned by gans,” *IEEE transactions on pattern analysis and machine intelligence*, 2020. [2](#)
- [21] E. Richardson, Y. Alaluf, O. Patashnik, Y. Nitzan, Y. Azar, S. Shapiro, and D. Cohen-Or, “Encoding in style: a stylegan encoder for image-to-image translation,” in *Proceedings of the IEEE/CVF Conference on Computer Vision and Pattern Recognition*, 2021, pp. 2287–2296. [2](#), [3](#), [5](#), [16](#)
- [22] T. Wang, Y. Zhang, Y. Fan, J. Wang, and Q. Chen, “High-fidelity gan inversion for image attribute editing,” in *Proceedings of the IEEE/CVF Conference on Computer Vision and Pattern Recognition*, 2022, pp. 11 379–11 388. [2](#), [3](#)
- [23] C. Shu, H. Wu, H. Zhou, J. Liu, Z. Hong, C. Ding, J. Han, J. Liu, E. Ding, and J. Wang, “Few-shot head swapping in the wild,” in *Proceedings of the IEEE/CVF Conference on Computer Vision and Pattern Recognition*, 2022, pp. 10 789–10 798. [2](#), [7](#)
- [24] O. Tov, Y. Alaluf, Y. Nitzan, O. Patashnik, and D. Cohen-Or, “Designing an encoder for stylegan image manipulation,” *ACM Transactions on Graphics (TOG)*, vol. 40, no. 4, pp. 1–14, 2021. [3](#), [5](#)
- [25] Y. Alaluf, O. Patashnik, and D. Cohen-Or, “Restyle: A residual-based stylegan encoder via iterative refinement,” in *Proceedings of the IEEE/CVF International Conference on Computer Vision*, 2021, pp. 6711–6720. [3](#)
- [26] X. Yao, A. Newson, Y. Gousseau, and P. Hellier, “Feature-style encoder for style-based gan inversion,” *arXiv e-prints*, pp. arXiv–2202, 2022. [3](#), [5](#), [16](#)
- [27] Yao, Xu and Newson, Alasdair and Gousseau, Yann and Hellier, Pierre, “A latent transformer for disentangled face editing in images and videos,” in *Proceedings of the IEEE/CVF international conference on computer vision*, 2021, pp. 13 789–13 798. [3](#)

- [28] R. Abdal, Y. Qin, and P. Wonka, "Image2stylegan: How to embed images into the stylegan latent space?" in *Proceedings of the IEEE/CVF International Conference on Computer Vision*, 2019, pp. 4432–4441. [3](#)
- [29] Abdal, Rameen and Qin, Yipeng and Wonka, Peter, "Image2stylegan++: How to edit the embedded images?" in *Proceedings of the IEEE/CVF Conference on Computer Vision and Pattern Recognition*, 2020, pp. 8296–8305. [3](#)
- [30] K. Kang, S. Kim, and S. Cho, "Gan inversion for out-of-range images with geometric transformations," in *Proceedings of the IEEE/CVF International Conference on Computer Vision*, 2021, pp. 13 941–13 949. [3](#)
- [31] R. Saha, B. Duke, F. Shkurty, G. W. Taylor, and P. Aarabi, "Loho: Latent optimization of hairstyles via orthogonalization," in *Proceedings of the IEEE/CVF Conference on Computer Vision and Pattern Recognition*, 2021, pp. 1984–1993. [3](#)
- [32] P. Zhu, R. Abdal, J. Femiani, and P. Wonka, "Barbershop: Gan-based image compositing using segmentation masks," *arXiv preprint arXiv:2106.01505*, 2021. [3](#)
- [33] J. Zhu, Y. Shen, D. Zhao, and B. Zhou, "In-domain gan inversion for real image editing," in *European conference on computer vision*. Springer, 2020, pp. 592–608. [3](#)
- [34] V. Blanz, K. Scherbaum, T. Vetter, and H.-P. Seidel, "Exchanging faces in images," in *Computer Graphics Forum*, vol. 23, no. 3. Wiley Online Library, 2004, pp. 669–676. [3](#)
- [35] D. Bitouk, N. Kumar, S. Dhillon, P. Belhumeur, and S. K. Nayar, "Face swapping: automatically replacing faces in photographs," in *ACM SIGGRAPH 2008 papers*, 2008, pp. 1–8. [3](#)
- [36] Y. Nirkin, I. Masi, A. T. Tuan, T. Hassner, and G. Medioni, "On face segmentation, face swapping, and face perception," in *2018 13th IEEE International Conference on Automatic Face & Gesture Recognition (FG 2018)*. IEEE, 2018, pp. 98–105. [3](#)
- [37] Nirkin, Yuval and Keller, Yosi and Hassner, Tal, "Fsganv2: Improved subject agnostic face swapping and reenactment," *IEEE Transactions on Pattern Analysis and Machine Intelligence*, vol. 45, no. 1, pp. 560–575, 2022. [3](#)
- [38] I. Korshunova, W. Shi, J. Dambre, and L. Theis, "Fast face-swap using convolutional neural networks," in *Proceedings of the IEEE international conference on computer vision*, 2017, pp. 3677–3685. [3](#)
- [39] J. Bao, D. Chen, F. Wen, H. Li, and G. Hua, "Towards open-set identity preserving face synthesis," in *Proceedings of the IEEE conference on computer vision and pattern recognition*, 2018, pp. 6713–6722. [3](#)
- [40] C. Xu, J. Zhang, M. Hua, Q. He, Z. Yi, and Y. Liu, "Region-aware face swapping," *arXiv preprint arXiv:2203.04564*, 2022. [3](#)
- [41] J. Kim, J. Lee, and B.-T. Zhang, "Smooth-swap: A simple enhancement for face-swapping with smoothness," in *Proceedings of the IEEE/CVF Conference on Computer Vision and Pattern Recognition*, 2022, pp. 10 779–10 788. [3](#)
- [42] E. Collins, R. Bala, B. Price, and S. Susstrunk, "Editing in style: Uncovering the local semantics of gans," in *Proceedings of the IEEE/CVF Conference on Computer Vision and Pattern Recognition*, 2020, pp. 5771–5780. [3](#)
- [43] M. J. Chong, W.-S. Chu, A. Kumar, and D. Forsyth, "Retrieve in style: Unsupervised facial feature transfer and retrieval," in *Proceedings of the IEEE/CVF International Conference on Computer Vision*, 2021, pp. 3887–3896. [3](#)
- [44] T. Park, M.-Y. Liu, T.-C. Wang, and J.-Y. Zhu, "Semantic image synthesis with spatially-adaptive normalization," in *Proceedings of the IEEE/CVF Conference on Computer Vision and Pattern Recognition*, 2019, pp. 2337–2346. [3](#), [6](#), [12](#)
- [45] P. Zhu, R. Abdal, Y. Qin, and P. Wonka, "Sean: Image synthesis with semantic region-adaptive normalization," in *Proceedings of the IEEE/CVF Conference on Computer Vision and Pattern Recognition*, 2020, pp. 5104–5113. [3](#), [10](#), [12](#)
- [46] A. Chen, R. Liu, L. Xie, Z. Chen, H. Su, and J. Yu, "Sofgan: A portrait image generator with dynamic styling," *ACM transactions on graphics*, 2021. [3](#), [6](#), [12](#)
- [47] T. Karras, S. Laine, and T. Aila, "A style-based generator architecture for generative adversarial networks," in *Proceedings of the IEEE/CVF conference on computer vision and pattern recognition*, 2019, pp. 4401–4410. [4](#), [9](#)
- [48] zllrunning, "face-parsing.pytorch," <https://github.com/zllrunning/face-parsing.PyTorch>, 2019. [4](#), [9](#)
- [49] P. Zhang, B. Zhang, D. Chen, L. Yuan, and F. Wen, "Cross-domain correspondence learning for exemplar-based image translation," in *Proceedings of the IEEE/CVF Conference on Computer Vision and Pattern Recognition*, 2020, pp. 5143–5153. [7](#)
- [50] S. Zhou, K. Chan, C. Li, and C. C. Loy, "Towards robust blind face restoration with codebook lookup transformer," *Advances in Neural Information Processing Systems*, vol. 35, pp. 30 599–30 611, 2022. [8](#), [10](#)
- [51] "Multi-band blending," https://github.com/BigRedT/Image_Blending. [8](#)
- [52] J. S. Kim, M.-K. Lee, and K.-S. Chung, "Image blending techniques based on gpu acceleration," in *Proceedings of the 2018 International Conference on Image and Graphics Processing*, 2018, pp. 106–109. [8](#)
- [53] A. Paszke, S. Gross, F. Massa, A. Lerer, J. Bradbury, G. Chanan, T. Killeen, Z. Lin, N. Gimelshein, L. Antiga *et al.*, "Pytorch: An imperative style, high-performance deep learning library," *Advances in neural information processing systems*, vol. 32, 2019. [9](#)
- [54] D. P. Kingma and J. Ba, "Adam: A method for stochastic optimization," *arXiv preprint arXiv:1412.6980*, 2014. [9](#)
- [55] H. Wang, Y. Wang, Z. Zhou, X. Ji, D. Gong, J. Zhou, Z. Li, and W. Liu, "Cosface: Large margin cosine loss for deep face recognition," in *Proceedings of the IEEE conference on computer vision and pattern recognition*, 2018, pp. 5265–5274. [11](#)
- [56] N. Ruiz, E. Chong, and J. M. Rehg, "Fine-grained head pose estimation without keypoints," in *The IEEE Conference on Computer Vision and Pattern Recognition (CVPR) Workshops*, June 2018. [12](#)
- [57] S. Gu, J. Bao, H. Yang, D. Chen, F. Wen, and L. Yuan, "Mask-guided portrait editing with conditional gans," in *Proceedings of the IEEE/CVF Conference on Computer Vision and Pattern Recognition*, 2019, pp. 3436–3445. [12](#)
- [58] Z. Wang, A. C. Bovik, H. R. Sheikh, and E. P. Simoncelli, "Image quality assessment: from error visibility to structural similarity," *IEEE transactions on image processing*, vol. 13, no. 4, pp. 600–612, 2004. [12](#)
- [59] M. Heusel, H. Ramsauer, T. Unterthiner, B. Nessler, and S. Hochreiter, "Gans trained by a two time-scale update rule converge to a local nash equilibrium," *Advances in neural information processing systems*, vol. 30, 2017. [12](#)
- [60] R. Zhang, P. Isola, A. A. Efros, E. Shechtman, and O. Wang, "The unreasonable effectiveness of deep features as a perceptual metric," in *Proceedings of the IEEE conference on computer vision and pattern recognition*, 2018, pp. 586–595. [16](#)
- [61] A. Krizhevsky, I. Sutskever, and G. E. Hinton, "Imagenet classification with deep convolutional neural networks," in *Advances in Neural Information Processing Systems*, F. Pereira, C. J. C. Burges, L. Bottou, and K. Q. Weinberger, Eds., vol. 25. Curran Associates, Inc., 2012. [Online]. Available: <https://proceedings.neurips.cc/paper/2012/file/c399862d3b9d6b76c8436e924a68c45b-Paper.pdf> [16](#)
- [62] —, "Imagenet classification with deep convolutional neural networks," *Advances in neural information processing systems*, vol. 25, 2012. [16](#)

- [63] R. Tzaban, R. Mokady, R. Gal, A. H. Bermano, and D. Cohen-Or, "Stitch it in time: Gan-based facial editing of real videos," *arXiv preprint arXiv:2201.08361*, 2022. 16

Appendix A. Training Objectives of the E4S Framework

RGI, the core of the proposed E4S, uses reconstruction as the proxy task, where we adopt the commonly used loss functions in the GAN inversion literature. Besides, the training objective of the proposed face re-coloring network B_ψ and face inpainting network P_τ will also be introduced here.

A.0.1. Loss for the RGI. Pixel-wise reconstruction loss. Defining the input image as I and the corresponding reconstructed image as \hat{I} , our pixel-wise reconstruction loss can be expressed as the Mean-Squared-Error (MSE):

$$\mathcal{L}_{mse} = \left\| \hat{I} - I \right\|_2^2 \quad (18)$$

Multi-scale LPIPS loss. Considering that pixel-wise reconstruction loss only cannot lead to a sharp result, inspired by [26], we additionally employ the multi-scale LPIPS [60] loss for a more sharp reconstructed result. The loss term is expressed as follows:

$$\mathcal{L}_{ms_lpipe} = \sum_s \left\| \mathbf{V}([\hat{I}]_s) - \mathbf{V}([I]_s) \right\|_2^2, \forall s \in \{256, 512, 1024\}, \quad (19)$$

where \mathbf{V} represents the AlexNet [61] feature extractor pre-trained on ImageNet [62] and $[I]_s$ represents the downsized input in resolution of s . This multi-scale perceptual loss allows the style codes to contain perceptual similarities at different levels.

Multi-scale face inversion loss. The previous work PSP [21] proposes an ID loss to maintain the input identity. Specifically, it leverages a pre-trained face recognition network, which encourages the cosine similarity between the input and the reconstructed face to be maximized. Besides, [26] further improve the ID loss with multi-scale form, which computing similarities in different feature levels. Following these two work, we define our multi-scale ID loss term as:

$$\mathcal{L}_{ms_id} = \sum_{i=1}^5 \left(1 - \langle R_i(I), R_i(\hat{I}) \rangle \right), \quad (20)$$

where $\langle \cdot \rangle$ denotes the cosine similarity and R is the pre-trained ArcFace [12] model.

Furthermore, following [26], we apply a multi-scale face parsing loss for a more accurate parsing, which can be expressed as:

$$\mathcal{L}_{ms_parsing} = \sum_{i=1}^5 \left(1 - \langle P_i(I), P_i(\hat{I}) \rangle \right), \quad (21)$$

where P is the pre-trained face parser [16].

Finally, our reconstruction loss \mathcal{L}_{recon} can be expressed as:

$$\mathcal{L}_{recon} = \mathcal{L}_{mse} + \lambda_1 \mathcal{L}_{ms_lpipe} + \lambda_2 \mathcal{L}_{ms_id} + \lambda_3 \mathcal{L}_{ms_parsing}, \quad (22)$$

where λ_1 , λ_2 , and λ_3 are trade-off hyperparameters.

Adversarial loss. Besides of the reconstruction loss \mathcal{L}_{recon} , we additionally use adversarial training to help improve the final image quality, which is expressed as:

$$\mathcal{L}_{adv} = \mathbb{E}[1 - \log D(\hat{I})] + \mathbb{E}[\log D(I)], \quad (23)$$

where D is initialized with the pre-trained StyleGAN discriminator. Finally, the overall loss function of our RGI is defined as:

$$\mathcal{L} = \mathcal{L}_{recon} + \lambda_{adv} \mathcal{L}_{adv}, \quad (24)$$

where the hyperparameters $\lambda_1, \lambda_2, \lambda_3$, and λ_{adv} are set as 0.8, 0.1, 0.1, and 0.01, respectively in all experiments.

A.0.2. Loss for the Face Re-coloring Network B_ψ . Reconstruction Loss. During training, given I'_A and I'_{AG} , the re-coloring network learns to predict the re-colored \tilde{I}^* . The predicted \tilde{I}^* should be fully consistent with the I_A (which equals to the flipped I'_A). To this end, we use a reconstruction loss consisting of an L2 loss and an LPIPS loss as the training objective:

$$\mathcal{L}_{\psi,rec} = \lambda_{\psi,1} \|I_A - \tilde{I}^*\|_2^2 + \lambda_{\psi,2} \|V(I_A) - V(\tilde{I}^*)\|_2^2, \quad (25)$$

where $\lambda_{\psi,1} = 1$ and $\lambda_{\psi,2} = 1$ can yield reasonable results without grid search in our experiments.

A.0.3. Details of Training the Face Inpainting Network P_τ . Training Settings and Loss Function. Similar to training re-coloring network B_ψ , training inpainting network P_τ requires paired data which is hard to collect. Therefore, we train P_τ in a self-supervised scheme. Given a face I , we generate random mismatch masks and edit its skin belonging to these mismatch regions based on the editing ability of our RGI method, obtaining an edited face I_{edit} . Then we take I_{edit} as the training input and I as the ground-truth supervision with a reconstruction loss:

$$\mathcal{L}_{\tau,rec} = \lambda_{\tau,1} \|I_A - \tilde{I}^*\|_2^2 + \lambda_{\tau,2} \|V(I_A) - V(\tilde{I}^*)\|_2^2, \quad (26)$$

where $\lambda_{\tau,1} = 1$ and $\lambda_{\tau,2} = 5$ in our experiments.

Appendix B. Video Face Swapping Results

The proposed E4S framework can be used to conduct video face swapping. Specifically, following STIT [63], we first crop and align the source image and the target video in advance, thus resulting in the source face S and an n -frame target face video $\{T_i\}_{i=1}^n$. Then, as described in Sec. 3.1 in our main paper, we can perform face re-enactment on the source S and make it have a similar pose and expression as each target frame. In this way, we can obtain a sequence of driven video $\{D_i\}_{i=1}^n$. Next, we can perform face swapping between each driven and target pair $\{(D_i, T_i)\}_{i=1}^n$.

Nonetheless, since our RGI is trained on images rather than videos, we find the above-mentioned video swapping results would have some temporal inconsistency. To deal with this, we turn to fine-tune the generator of our RGI on

all the driven frames, where the \mathcal{L}_{recon} is the loss function. The parameters are updated 200 times for each frame, where the learning rate is 10^{-3} . After finetuning, we still adopt the frame-by-frame swapping strategy to obtain a temporally consistent result.

We compare our results with FaceShifter [9] and HiRes [3] in Fig. 13, where the whole video is on our project page. HiRes struggles to generate a wink in the swapped video. Besides, FaceShifter sometimes fails to transfer the source identity. As contrast, our results show better visual quality and temporal consistency.

Appendix C.

User-interface System For Image and Video Face Swapping

We develop a user-interface system to perform image and video face swapping. A screenshot is shown in Fig. 14. Given a source image and a target image or video, our user-interface system can produce a high-quality swapped image or video. An interactive face swapping demo can also be found on our project page.

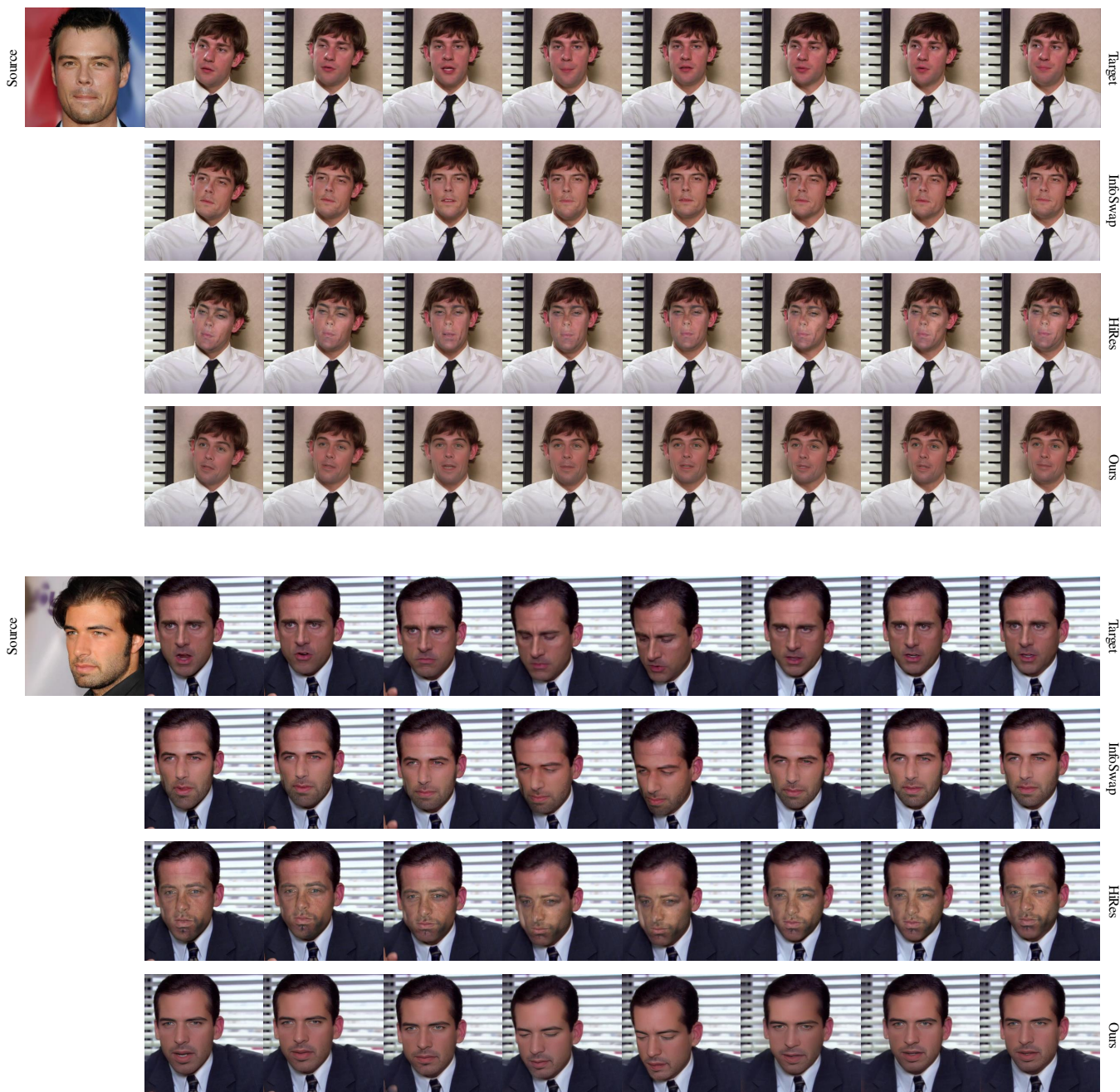


Figure 13: Video face swapping comparisons of our results with FaceShifter [9] and HiRes [3]. Our method shows the better capability of source identity transferring and target attribute preservation (e.g., pose, expression, wink, lighting). Their visual quality and temporal consistency also inferior to our method.

E4S: Fine-Grained Face Swapping via Regional GAN Inversion

Image Video

source image



target video



result



0:00 / 0:00

Run

Advanced Video Swapping Options

Target Max Frames Count (-1: use all frames)

Crop Inputs? (crop and align the faces)

Enable PTI Tuning (finetuning the generator to obtain more stable video result)

Advanced PTI Tuning Options

Max PTI Steps

PTI Learning Rate

Recolor Lambda

PTI Resume Weight Path

Figure 14: A screenshot of our interactive image and video face swapping system. The button in the upper left corner can choose whether to swap face in images or videos.